Modulation Linearity Characterization of Si Mach-Zehnder Modulators

Min-Hyeok Seong, *Graduate Student Member, IEEE*, Yongjin Ji, Chul-Soon Im, Youngseok Bae, and Woo-Young Choi, *Member, IEEE*

***Abstract*—Linearity of Si Mach-Zehnder Modulators (MZM) is characterized with a newly-proposed modeling technique which includes the influences of the transmission characteristics of traveling-wave (TW) electrodes and the electro-optic (EO) characteristics of PN junction phase shifters within Si MZMs. Using the technique, the third-order intermodulation distortion (IMD3) and the spurious-free dynamic range (SFDR) of a sample Si MZM device are determined, and their accuracy is verified with measurement results. In addition, the contributions of different nonlinear parameters to the nonlinearity of the sample Si MZM are identified.**

***Index Terms*—Intermodulation distortion, Microwave photonics, Modulation linearity, Si Mach-Zehnder modulators, Spurious free dynamic range.**

I. Introduction

HIGH-PERFORMANCE optical modulators are extremely important for many applications. They are one of the key building blocks for present-day optical communication systems, for which many different types of modulators are available [1].

For applications in the fields of microwave photonics that include radio-over-fiber transmission systems [2], [3], [4], photonic microwave filters [5], and photonic analog-to-digital converters [6], [7], optical modulators are used for converting high-frequency electrical signals into the optical domain, and for this, linearity of the optical modulator is one of the key device characteristics that greatly affect the entire system performance. In particular, the third-order intermodulation distortion (IMD3) and its influence on the spurious-free dynamic range (SFDR) are often used for the modulator performance metrics.

In this article, we investigate the modulation linearity of the Si-based Mach-Zehnder modulators (MZM). Utilizing the powerful Si fabrication technology, Si photonics can offer advantages of the high integration level at the low cost for many photonic systems including microwave photonics [8]. Accurate characterization of the linearity of Si optical modulators is essential for understanding the influences of the device characteristics on the entire system performance and finding ways for their enhancement. Recent studies have reported linearity characteristics of Si MZMs based on simulation [9] and measurement [10]. Furthermore, various device design optimization techniques have been proposed for improving Si MZM linearity characteristics [11], [12], [13].

Previously reported techniques of Si MZM linearity characterization include the Taylor expansion of the transfer function [9], but complex mathematical expressions used in this technique make it challenging to apply them in practice. In [14], analytical expressions are derived for the second- and third-order harmonic distortions but the discrepancy between calculation and measurement is not clearly explained. In [15], the optimal operating conditions for the largest SFDR of the Si MZM were reported but it did not provide a modeling technique with which the Si MZM linearity performance can be predicted.

In this article, we attempt to develop a comprehensive linearity modeling technique for Si MZMs. Our model includes the influences of characteristics of the phase shifters as well as the traveling-wave (TW) electrodes. The numerical values for the model parameters are extracted from either measurement or simulation. The IMD3 and the SFDR for a sample Si MZM are determined with this modeling technique and successfully verified with the measurement results. The microwave frequency range of interest for the present investigation is the X band around 10 GHz, but our technique can be applied to other frequency ranges of interest.

This article is organized as follows. Section II explains our technique of modeling Si MZM linearity characteristics. Section III shows the structure and the key characteristics of the sample Si MZM that is used for verifying the accuracy of our technique. Section IV describes the extraction of the parameters of the Si MZM and the experimental verification of the parameters using measurement results of electro-optic (EO) response. Section V compares the modeling results with the measurement results. Section VI analyzes effects of various parameters on the Si MZM linearity, and Section VII concludes this article.

II. Si MZM Linearity Model

A Si MZM is composed of TW electrodes for delivering microwave signals and PN-junction-based Si waveguides for

Manuscript received 28 June 2023; revised 27 September 2023; accepted 19 October 2023. Date of publication 24 October 2023; date of current version 18 March 2024. This work was supported by the Agency for Defense Development of the Korean Government under Grant UD210032TD. *(Corresponding author: Woo-Young Choi.)*

Min-Hyeok Seong, Yongjin Ji, and Woo-Young Choi are with the High-Speed Circuits and Systems Laboratory, Department of Electrical and Electronic Engineering, Yonsei University, Seoul 03722, South Korea (e-mail: alsguree@yonsei.ac.kr; yjji0314@yonsei.ac.kr; wchoi@yonsei.ac.kr).

Chul-Soon Im is with the Hanwha Systems Company, Ltd. Yongin R&D Center, Yongin-Si 17122, South Korea (e-mail: chulsoonim@hanwha.com).

Youngseok Bae is with the Agency for Defense Development, Daejeon 34186, South Korea (e-mail: youngseok.bae@add.re.kr).

Color versions of one or more figures in this article are available at https://doi.org/10.1109/JLT.2023.3327146.

Digital Object Identifier 10.1109/JLT.2023.3327146

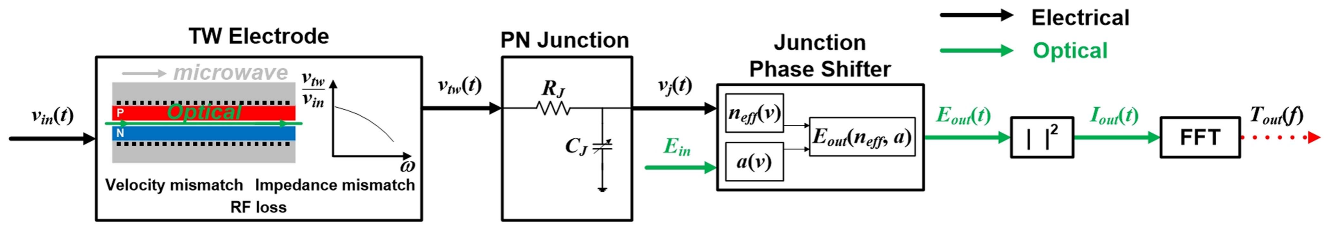

Fig. 1. Block diagram of the linearity simulation model of Si MZM in this research.

optical signal propagation. The microwave signals propagating on the TW electrodes induce an EO modulation by changing the depletion width of the PN junction, carrier injection, or carrier accumulation within the Si waveguide. The linearity characteristics of the Si MZMs are influenced by several factors: the nonlinear dependence on the bias voltage of both the Si waveguide effective index and the junction capacitance, and the transmission-line characteristics of the TW electrodes.

Fig. 1 shows the sequence in which above three factors are considered in our investigation. When $v_{in}(t)$, a sinusoidal voltage signal having angular frequency ω, is applied to a Si MZM, it goes through the TW electrodes to reach the Si waveguide, but there is a certain amount of modification in the signal level due to impedance mismatch between source, load, and TW electrode characteristic impedances; velocity mismatch between light and RF signals; and RF loss in TW electrodes. [16] and [17] model the average voltage, $v_{avg}(\omega)$, experienced by the light on the TW electrode, after $v_{in}(t)$ experiences the above-mentioned three factors, with the following equation,

$$v_{avg}(\omega) = v_g \cdot \frac{\exp(j\beta_o(\omega)L_{tw}) \cdot (1+\Gamma_g(\omega)) \cdot (V_+(\omega)+\Gamma_l(\omega) \cdot V_-(\omega))}{\exp(j\beta_e(\omega)L_{tw})+\Gamma_l(\omega) \cdot \Gamma_g(\omega) \cdot \exp(-j\beta_e(\omega)L_{tw})} \tag{1}$$

In the above equation, v_g is the amplitude of $v_{in}(t)$. L_{tw} is the length of the TW electrode. Γ_g and Γ_l are the reflection coefficients at the load and the source, respectively, and are given as

$$\Gamma_l(\omega) = \frac{Z_L - Z_o(\omega)}{Z_L + Z_o(\omega)}, \quad \Gamma_g(\omega) = \frac{Z_o(\omega) - Z_g}{Z_o(\omega) + Z_g}. \tag{2}$$

Z_o is the characteristic impedance of the TW electrode. Z_L is the load resistance. Z_g is the impedance of the microwave source, which is 50 Ω in this study. V_+ and V_- are expressed as [16], [17]

$$V_\pm(\omega) = \exp\left(\pm j\frac{\beta_e(\omega) \mp \beta_o(\omega)}{2}L_{tw}\right) \cdot \frac{\sin\left(\frac{\beta_e(\omega)\mp\beta_o(\omega)}{2}L_{tw}\right)}{\frac{\beta_e(\omega)\mp\beta_o(\omega)}{2}L_{tw}}, \tag{3}$$

where β_o and β_e are the propagation constants of the optical and the microwave signal, respectively, which are given as

$$\beta_o(\omega) = \frac{\omega}{c}n_o, \beta_e(\omega) = -j\left(\alpha(\omega) + j\frac{\omega}{c}n_{mw}(\omega)\right) \tag{4}$$

Here, α and n_{mw} are the attenuation coefficient and the refractive index of the TW electrode for the microwave signals, respectively. n_o is the group index of the optical signal passing through the PN-doped Si waveguide.

When an external sinusoidal signal $v_{in}(t)$ is applied to the electrode, the influence of the TW electrode can be modeled with $v_{tw}(t)$ given as

$$v_{tw}(t) = v_{in}(t) \cdot \left|\frac{v_{avg}(\omega)}{v_{avg}(0)}\right| \tag{5}$$

which represents $v_{in}(t)$ modified with the scaling factor determined by the TW effect. As can be seen in (5), when ω of $v_{in}(t)$ is small there is little TW effect, but when ω is large the voltage experienced by the light can be significantly different from $v_{in}(t)$.

As can be seen in Fig. 1, $v_{tw}(t)$ is further influenced by the junction resistance, R_J, and voltage-dependent junction capacitance, C_J, of the Si waveguide. $v_j(t)$, the actual voltage signal applied to the PN-doped Si waveguide, causes changes in $n_{eff}(v)$, the Si waveguide effective refractive index, and $a(v)$, the optical absorption coefficient of the Si waveguide, due to the plasma dispersion effect. Then, assuming that the voltage signals are applied to the Si MZM at zero bias voltage in the differential manner, $E_{out}(t)$, the Si MZM output electric field, can be expressed as

$$E_{out} = \frac{1}{2} \cdot E_{in} \cdot \left[j \cdot \exp(-a(-v_j/2)L_m) \cdot \exp\left(-j\frac{2\pi n_{eff}(-v_j/2)}{\lambda}\right)L_m \cdot \exp(-j\phi) + \exp(-a(v_j/2)L_m) \cdot \exp\left(-j\frac{2\pi n_{eff}(v_j/2)}{\lambda}\right)L_m\right]. \tag{6}$$

Here, L_m is the length of the PN junction phase shifter. ϕ is the initial optical phase difference between two arms of the Si MZM. The intensity of the modulated optical signal, $I_{out}(t)$, can be obtained from $E_{out}(t)$, and this can be converted into the power spectral density, $T_{out}(f)$, from which the IMD3 of the Si MZM can be determined.

III. Si Single-Ended Push-Pull MZM

In order to verify the accuracy of the above-explained linearity modeling technique, a Si single-ended push-pull MZM (SPPMZM) [18], whose structure is shown in Fig. 2(a), is fabricated by a Si photonics foundry. Modulation type of the Si SPPMZM is depletion type, which means that EO modulation is generated by the change of the depletion region. In the Si SPPMZM, PN diodes are connected in series. With this, the junction capacitance is reduced approximately by half compared to the structure having one PN diode, but the resistance does not increase twice because of the non-negligible resistance from

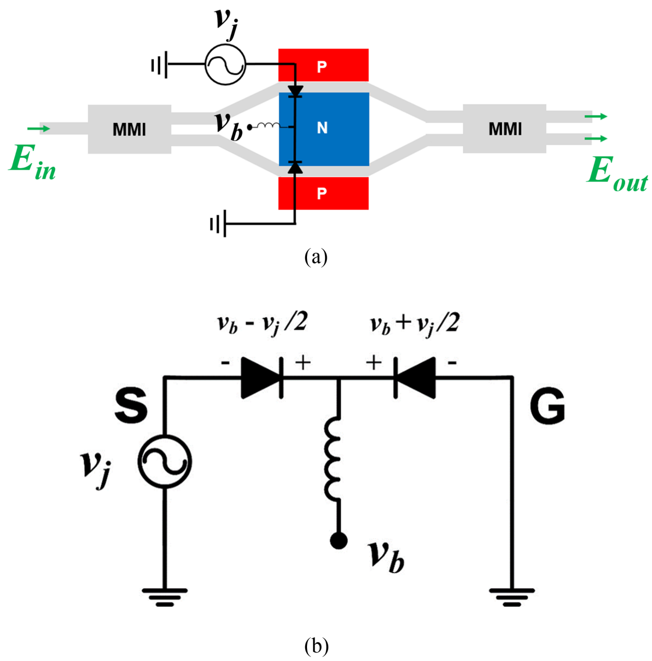

Fig. 2. (a) Block diagram of the structure of the Si SPPMZM and (b) equivalent DC circuit schematic of modulation section of the Si SPPMZM.

about 13.5-μm long Si layers between the electrode and two PN junctions which remains the same. This results in the reductions of both RC time constant and RF loss of the TW electrode, which lead to higher modulation bandwidth. A 1×2 multimode interferometer (MMI) is used for dividing the input optical signal into two and a 2×2 MMI mixes two signals that have traveled two different phase shifters. A reverse bias voltage, v_b, is applied to the common N-region of two phase shifters through an inductor. The external inductor which has a high inductance of 546 μH provided by a commercial Bias-T prevents the RF signal from propagating on the bias line, which makes sure that the Si SPPMZM has the push-pull operation. When the microwave signal, v_j, is applied to one of two P-regions designated as S, it sees two capacitors in series and, as a result, $v_b - v_j/2$ is applied to one PN junction and $v_b + v_j/2$ to another PN junction. Thus, the Si SPPMZM modulates the optical signal in the differential manner with a single RF input as shown in Fig. 2(b).

The chip photograph of the fabricated Si SPPMZM is shown in Fig. 3(a). The target wavelength band is C band. The device has 2-mm PNP-doped junction phase shifters and a 2.4-mm TW electrode, whose characteristic impedance is designed to be 50 Ω. A termination resistor is added at the end of the TW electrode. Thermo-optic heaters are added to both arms of the Si SPPMZM, so that the bias point can be thermally tuned. Grating couplers are used for optical I/O. Fig. 3(b) displays the vertical cross-sectional view of the junction phase shifters in the Si SPPMZM.

IV. Extraction of The Model Parameters

Numerical values for the model parameters of our linearity model should be determined for the Si SPPMZM so that accurate

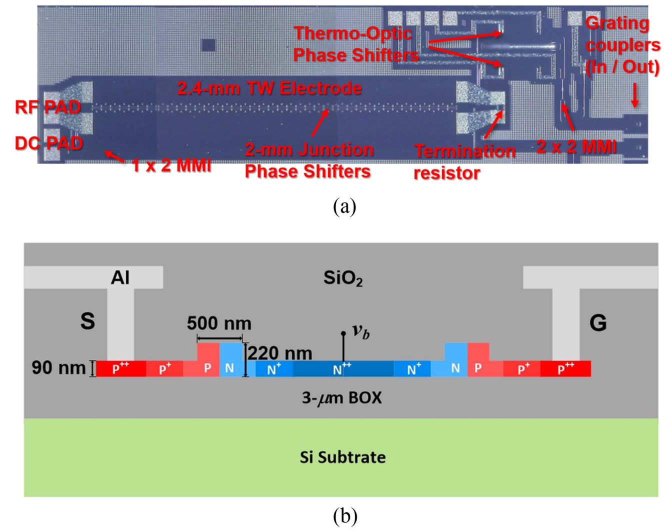

Fig. 3. (a) Microphotograph of the fabricated Si SPPMZM and description of each part and (b) cross-section diagram of the junction phase shifters of the Si SPPMZM.

linearity characterization can be performed. Details of how they are extracted are explained below.

A. n_{eff} and a

Because details of doping concentrations for the junction phase shifters are not provided by the foundry, the numerical values for $n_{eff}(v)$ and $a(v)$ are determined by measuring the sample Si SPPMZM transmission characteristics and fitting the results based on the model to the measurement results. In the measurement, we intentionally apply v_b to only one of the PN diodes in the Si SPPMZM. Then, the resulting transmission characteristic is modified from (6) as

$$
\begin{aligned}
E_{out} &= \frac{1}{2} \cdot E_{in} \\
&\cdot \left[j \cdot \exp(-a(v_b)L_m) \cdot \exp\left(-j\frac{2\pi n_{eff}(v_b)}{\lambda}\right) L_m \cdot \exp(-j\phi) \right. \\
&\left. + \exp(-a(0)L_m) \cdot \exp\left(-j\frac{2\pi n_{eff}(0)}{\lambda}\right) L_m \right]. \qquad (7)
\end{aligned}
$$

As doping information is not available in process design kit (PDK) of the Si foundry, we first estimate the effective doping concentrations of P/N regions assuming they are uniformly doped using the values of the sheet resistances given in the PDK first. Since they are not accurate enough, we fine-tune them until the simulated $n_{eff}(v)$ with the effective doping concentrations agree with the measured $n_{eff}(v)$ obtained at 1550 nm. For simulation, Ansys's Lumerical is used. Fig. 4(a) shows the measurement results at 1550 nm. As v_b increases, the depletion region in the PN junction becomes wider, resulting in decrease in a and increase in n_{eff}. Fig. 4(b) shows comparison between the measured and simulated n_{eff} values at different bias voltages. The estimated effective uniform doping concentrations of P/N regions are P: 6×10^{17} cm^{-3} and N: 4×10^{17} cm^{-3}. Fig. 5 represents the measured data (dotted lines) and the simulated

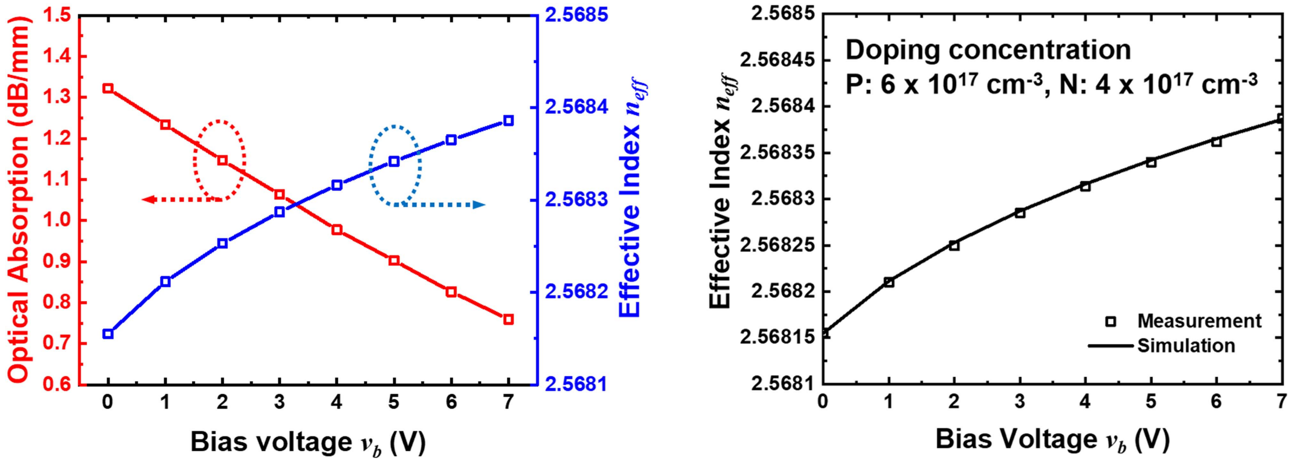

(a) (b)

Fig. 4. (a) Extracted optical absorption coefficient a and effective refractive index n_{eff} of the junction phase shifter in the Si SPPMZM at 1550 nm and (b) extracted n_{eff} from the measurement and simulated n_{eff} at doping concentrations of P: 6×10^{17} cm^{-3} and N: 4×10^{17} cm^{-3}.

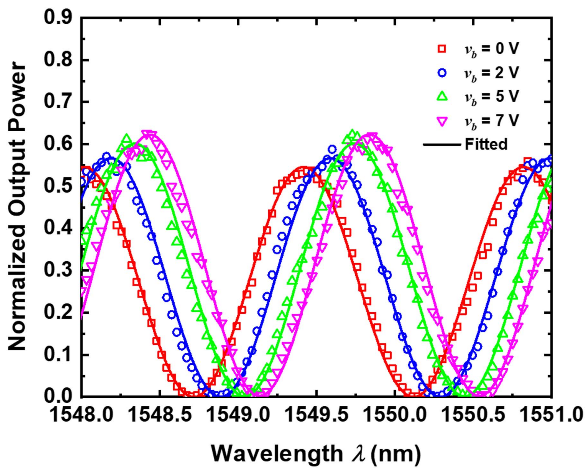

Fig. 5. Measured and fitted values of normalized optical transmission spectra with various v_b.

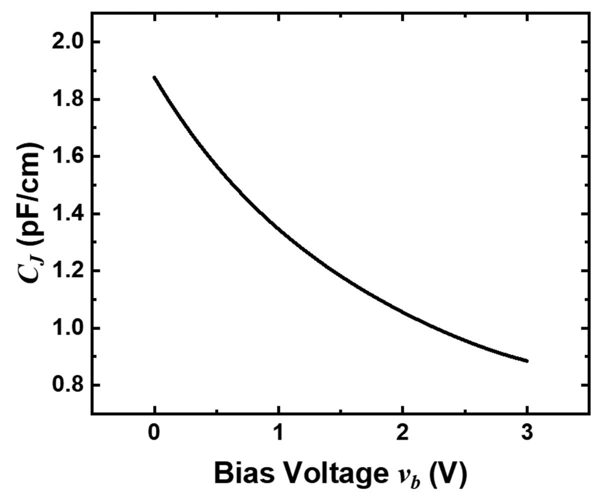

Fig. 6. Simulated C_J based on the extracted doping concentrations along v_b.

results (solid lines) of the normalized MZM transmission characteristics. For the simulation, the influence of the Si waveguide dispersion is included by using $dn_{eff}/d\lambda$ of $-0.885\ \mu\text{m}^{-1}$ for the PN doped waveguide in the junction phase shifters and $-1.18\ \mu\text{m}^{-1}$ for other undoped waveguide, both of which are determined from simulation. a is also a wavelength-dependent parameter, but, according to simulation, it is negligible for the wavelength range of interest.

B. Z_o, n_{mw}, α, n_o, and Z_L

Z_o, n_{mw} and α are related to the transmission characteristics of the TW electrode. These three parameters can be determined from the electromagnetic simulation. Since the Si PNP junction influences the transmission characteristics of the TW electrode, it is necessary to determine R_J and C_J for the sample Si SPPMZM. R_J and C_J can be determined from the PN junction with the extracted doping concentrations. Fig. 6 shows the estimated values of C_J with device simulation of Lumerical. R_J is estimated to be 1.5 Ω·cm regardless of the bias voltage by I-V simulation of Lumerical. For the I-V simulation, we determine the effective doping concentrations corresponding to various Si layers using the sheet resistance information provided in the PDK.

With these estimated values for R_J and C_J along with the TW electrode used in the Si SPPMZM, an electromagnetic simulation is carried out with Keysight's Advanced Design System. Fig. 7(a) and (b) show the simulated electrical S21 and S11 parameters at different v_b. From these, Z_o, n_{mw}, and α can be determined [19], [20], and the results are shown in Fig. 8(a), (b), and (c) for different v_b. As shown in Fig. 8(a), Z_o is slightly lower than 50 Ω. This is due to the fact that the precise values of R_J and C_J are not known at the time of designing the Si SPPMZM device.

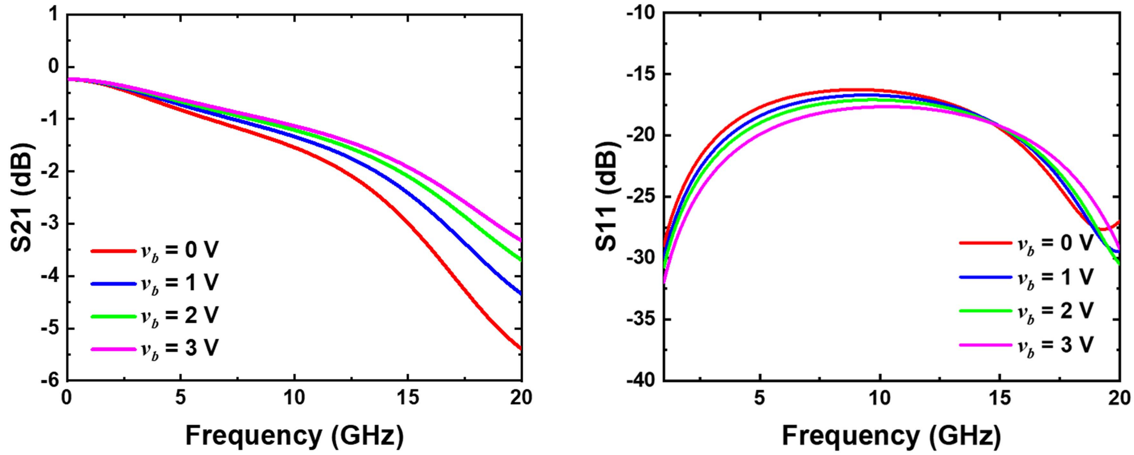

(a) (b)

Fig. 7. (a) Electrical S21 and (b) S11 from an electromagnetic simulation of the TW electrode of the Si SPPMZM.

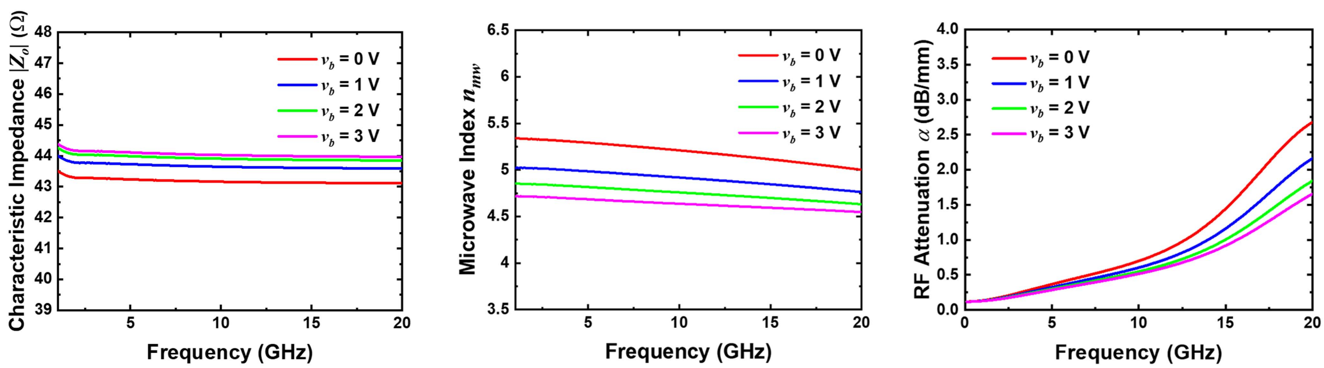

(a) (b) (c)

Fig. 8. (a) Magnitude of characteristic impedance $|Z_o|$, (b) microwave index n_{mw} and (c) RF attenuation α of the TW electrode obtained from the simulated electrical S parameters.

Meanwhile, n_o is determined with the mode simulation for the waveguide having the estimated uniform doping concentrations, and the value of 3.94 is obtained. Z_L of 50.8 Ω is also determined by I-V measurement with the termination resistor.

C. Confirmation of Accuracy of Extracted Parameters

In order to confirm the accuracy of the extracted model parameter values, EO frequency response, $S_{21.E\text{-}O}(\omega)$, is measured for different values of v_b and is compared with the calculated results with the extracted model parameter values.

The dotted data in Fig. 9 shows the measurement results. $S_{21.E\text{-}O}(\omega)$ can be determined from the equation given as [21]

$$S_{21.E-O}(\omega) = \frac{1}{\sqrt{(\omega R_J C_J)^2 + 1}} \cdot \left| \frac{v_{avg}(\omega)}{v_{avg}(0)} \right| \tag{8}$$

The solid lines in Fig. 9 shows the calculated $S_{21.E\text{-}O}(\omega)$ using the extracted numerical values for the model parameters. The agreement is reasonable indicating those extracted parameter values can be used for Si MZM linearity analysis. As shown in Figs. 7(a) and 9, it can be observed that the RF frequency at which electrical S21 reaches −6.4 dB does not coincide with the frequency at which EO S21 reaches −3 dB. This disparity can be attributed to the velocity mismatch between optical and RF signals and impedance mismatch between source, load, and the TW electrodes [22]. C_J and R_J also affect EO S21, so that the disparity can be larger.

V. Linearity Simulation and Measurement

Fig. 10 shows the setup used in the IMD3 measurement of the sample Si SPPMZM for the verification of the proposed linearity simulation model. We use two RF sources (Anritsu 68177C and Agilent 83752B) and a power combiner (Mini-Circuits ZX10-2-183-S+) for inputting two-tone signal to the Si MZM. Optical receiver (Optilab PR-23-M) is used for converting optical signal to electrical signal, and RF spectrum analyzer (Agilent 8593E) is used for obtaining RF power spectrum density. For both simulation and measurement, two-tone sinusoidal signals having 9.9-GHz and 10.1-GHz frequencies are introduced into the

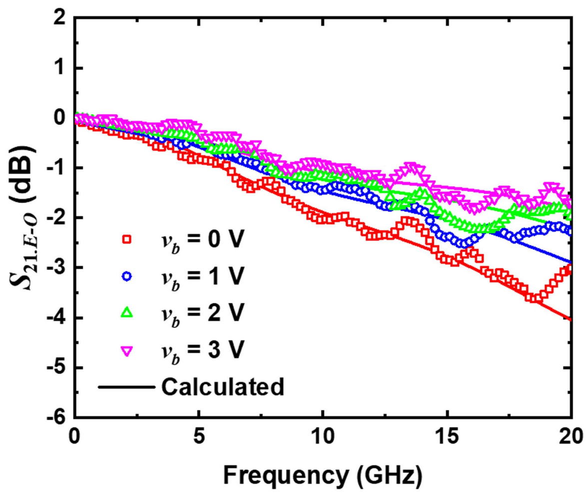

Fig. 9. Normalized values of the EO S21 of the Si SPPPMZM from measurement (dotted values) and calculation (solid lines).

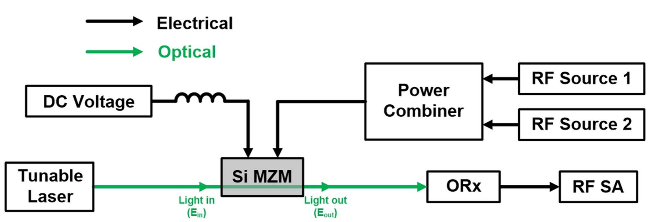

Fig. 10. Setup used in measurement of the Si SPPMZM linearity for the verification of the linearity simulation model. ORx: optical receiver, RF SA: RF spectrum analyzer.

device. The simulated $T_{out}(f)$ is obtained based on the process shown in Fig. 1 using the extracted parameter values. To experimentally validate the simulation results, $T_{out}(f)$ is measured. The wavelength used in the measurement is 1548.8 nm, because the least coupling loss is caused by the grating couplers at this wavelength. The optical power introduced into the Si SPPMZM is 0 dBm. For the measurement, the Si SPPMZM is placed on a stage whose temperature is controlled at 25 °C.

Fig. 11(a) shows the simulated $T_{out}(f)$ spectrum (solid lines) as well as the measured results (empty squares). The 9.9-GHz and 10.1-GHz signals are the fundamental components, while 9.7-GHz and 10.3-GHz signals are the IMD3 components. Fig. 11(b) represents the results of the simulation and the measurement for the fundamental and IMD3 components with the varying v_b when the Si SPPMZM is at the Q point, where the half of the input light is transmitted. The results from the simulation and the measurement match well, having the difference of no more than 1.5 dB. In addition, the simulation and the measurement results are compared at different bias points achieved with the phase difference provided by the thermo-optic heaters. Fig. 12(a), (b), (c) and (d) show the results at different v_b values. As can be seen in the figures, the results of the simulation and the measurement illustrate well agreement with each other. The simulated results in Fig. 12 depict that the ratio of the IMD3 power to the fundamental power has little dependance on the bias points whereas the measurement results show some improvement as the bias point moves away from the Q point. This may be due to the limitation in our model.

The noise floor estimation should be preceded before the SFDR determination [23]. Relative intensity noise (RIN) of −140 dB/Hz is used for the tunable laser, and the temperature of 25 °C is used for thermal noise calculation. The bandwidth for the noise calculation is 1 Hz. For example, at Q point and $v_b = 1$ V, an input optical power of 0 dBm becomes −5.5 dBm at output of the Si SPPMZM. This generates a photocurrent of 0.184 mA with the 0.65-A/W photodetector of the optical receiver used in the measurement. This photocurrent leads to shot and RIN noise of −175.3 dBm and −167.7 dBm, respectively. The thermal noise generated by temperature is −173.9 dBm, and as a result, the total noise is −166.1 dBm. After including the transimpedance gain of 1150 V/A in the optical receiver, the noise floor can be assumed to be −138.9 dBm/Hz.

The simulation and the measurement are performed with the increasing input RF power for the SFDR determination. Microwave signals ranging from −4 dBm to 10 dBm are used for the simulation, while input signals ranging from 6 dBm to 10 dBm are used for the measurement. Measurement for lower input power was not possible due to the sensitivity limitation of the RF spectrum analyzer used in the measurement. Fig. 13(a) and (b) show the results of fitting the fundamental and IMD3 signals for simulation and measurement at the Q bias with v_b = 1 V. Fig. 13(c) shows the measured and simulated SFDR values for different v_b values at the Q bias. Even when v_b and ϕ are changed, the simulated values of the SFDR show a very small difference compared to the measured values. The SFDR values have a small variation with v_b, because if v_b becomes larger, the noise floor becomes higher while the IMD3 decreases.

VI. Linearity Analysis With Parameters of Si MZM

With the confirmation of the accuracy of our Si MZM linearity model, it is now possible to run simulation with controlled parameter inputs and determine the contribution of key device parameters toward modulation nonlinearity. The device parameters that strongly influence Si MZM nonlinearity are n_{eff} and C_J. Fig. 14(a) shows the simulated ratio between the IMD3 and fundamental signal power at Q point assuming linear n_{eff} and compares the results with the real case. As can be seen in the figure, there is a significant difference between these two cases when v_b is small. Fig. 14(b) shows the simulated ratio between the IMD3 and fundamental power at Q point assuming constant C_J and compares the results with the real case. The difference between the two cases becomes larger when v_b is larger. These results indicate that n_{eff} gives the major contribution to the linearity of the Si SPPMZM when v_b is small, while C_J has larger impact when v_b is large.

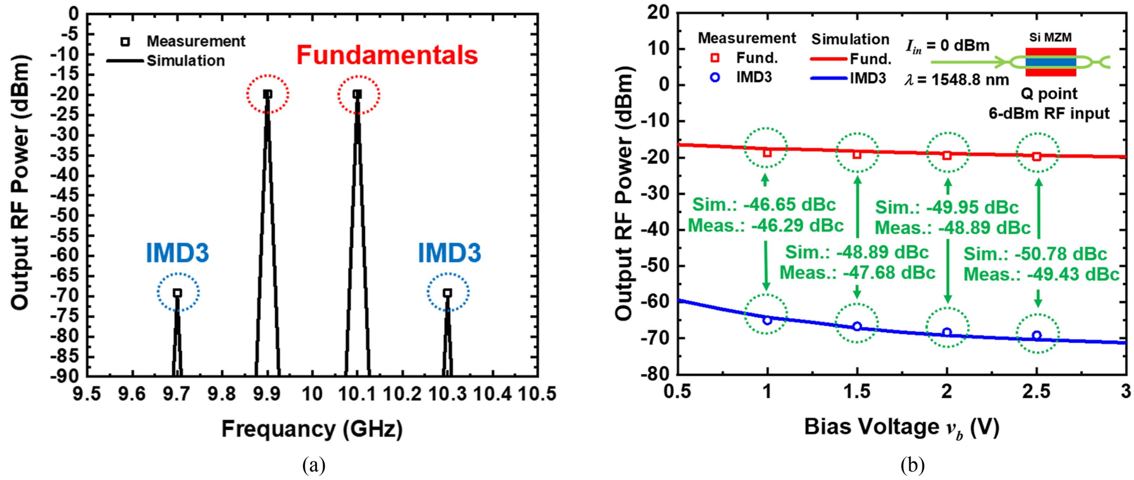

Fig. 11. (a) Fundamental and IMD3 components generated by 9.9-GHz and 10.1-GHz microwave input and (b) simulated and measured values of fundamental and IMD3 signals along v_b. The input optical power applied to the Si SPPMZM is 0 dBm. The used wavelength is 1548.8 nm. Input RF power is 6 dBm. The bias point is Q point.

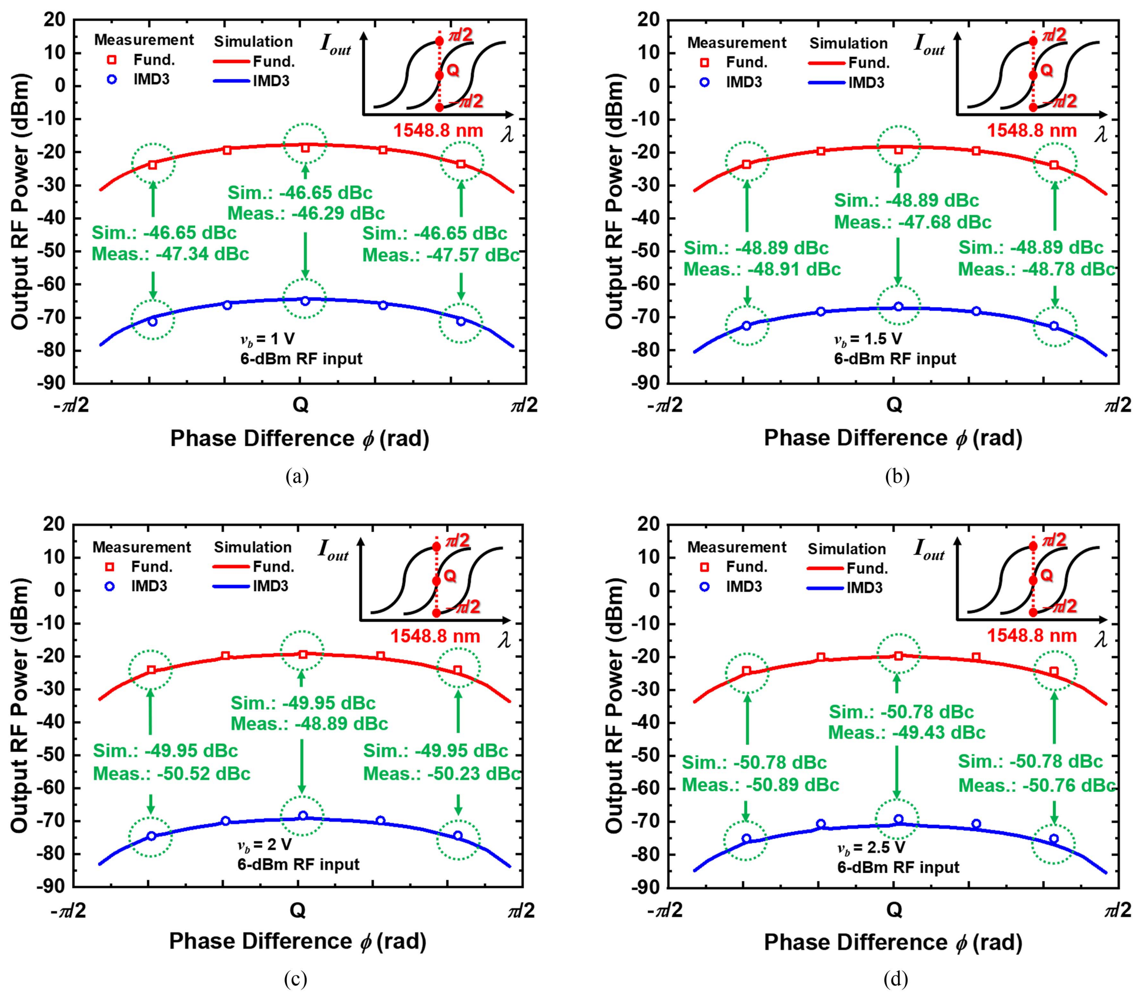

Fig. 12. Simulated and measured values of fundamental and IMD3 power along ϕ at (a) $v_b = 1$ V, (b) $v_b = 1.5$ V, (c) $v_b = 2$ V and (d) $v_b = 2.5$ V. The input optical power applied to the Si SPPMZM is 0 dBm. The used wavelength is 1548.8 nm. The input RF power is 6 dBm.

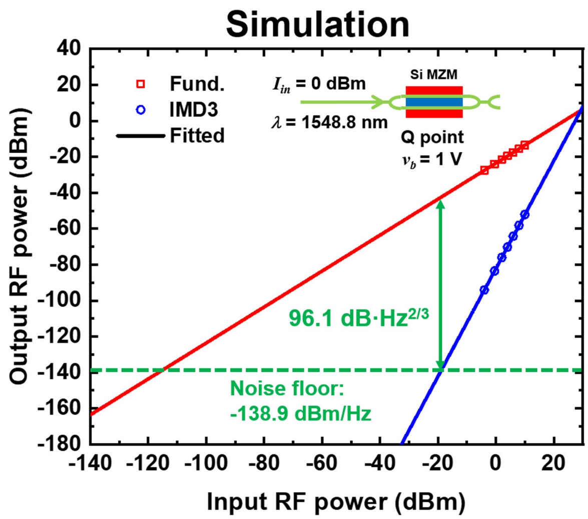

(a)

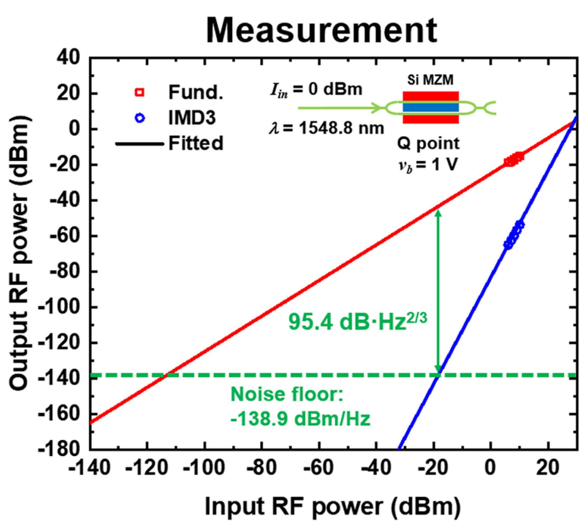

(b)

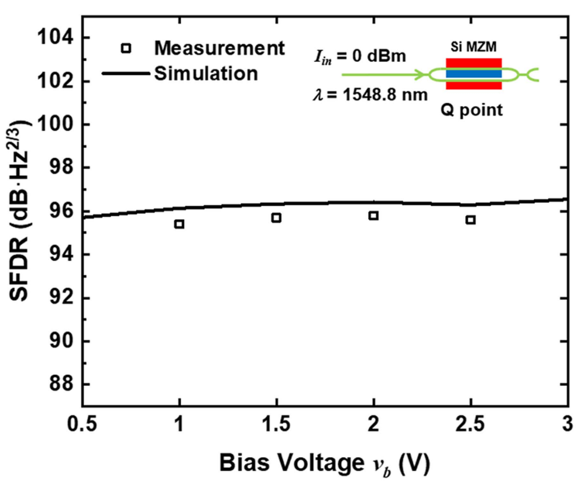

(c)

Fig. 13. (a) Simulated output RF power of fundamental and IMD3 signals, and SFDR value by the proposed model and (b) those measured from setup described in Fig. 10. (c) SFDR values along different v_b at Q point. The input optical power applied to the Si SPPMZM is 0 dBm. The used wavelength is 1548.8 nm.

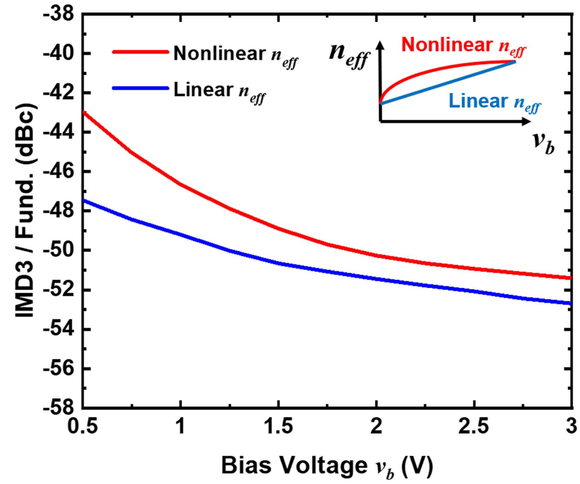

(a)

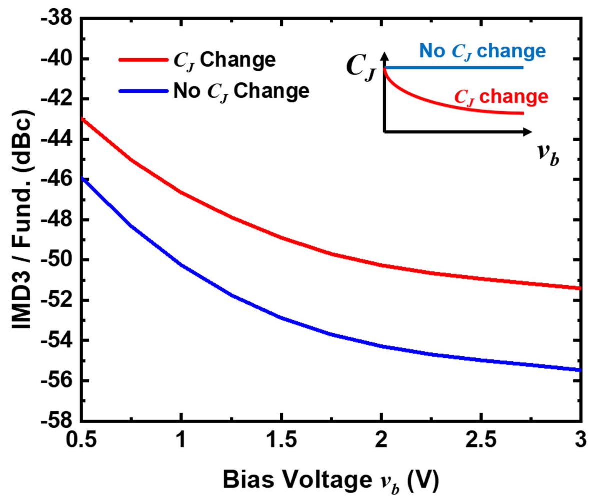

(b)

Fig. 14. Simulated ratio between the RF power of fundamental and IMD3 signals at Q point, (a) when n_{eff} is linear or not and (b) when C_J is changed or not.

VII. Conclusion

We presented a new modeling technique with which the linearity characteristics of Si MZM can be precisely analyzed. Our model includes the effects of the optical characteristics of the junction phase shifters as well as the transmission characteristics of the TW electrodes. Using this modeling technique, IMD3 and SFDR characteristics of a sample Si MZM device is determined, and their accuracies are confirmed with the measurement results. This technique should be very useful for designing optimized Si MZM especially for analog applications for which the Si MZM linearity is very important.

References

[1] G. Sinatkas, T. Christopoulos, O. Tsilipakos, and E. E. Kriezis, "Electro-optic modulation in integrated photonics," *J. Appl. Phys.*, vol. 130, no. 1, Jul. 2021, Art. no. 010901, doi: 10.1063/5.0048712.

[2] T. Kurniawan, A. Nirmalathas, C. Lim, D. Novak, and R. Waterhouse, "Performance analysis of optimized millimeter-wave fiber radio links," *IEEE Trans. Microw. Theory Techn.*, vol. 54, no. 2, pp. 921–928, Feb. 2006, doi: 10.1109/TMTT.2005.863047.

[3] C. Lim, A. Nirmalathas, K. Lee, D. Novak, and R. Waterhouse, "Intermodulation distortion improvement for fiber–radio applications incorporating OSSB+C modulation in an optical integrated-access environment," *J. Lightw. Technol.*, vol. 25, no. 6, pp. 1602–1612, Jun. 2007, doi: 10.1109/JLT.2007.896814.

[4] D. Novak et al., "Radio-over-fiber technologies for emerging wireless systems," *IEEE J. Quantum Electron.*, vol. 52, no. 1, Jan. 2016, Art. no. 0600311, doi: 10.1109/JQE.2015.2504107.

[5] A. M. Gutierrez et al., "A photonic microwave filter based on an asymmetric silicon Mach-Zehnder modulator," *IEEE Photon. J.*, vol. 5, no. 4, Aug. 2013, Art. no. 5501006.

[6] G. C. Valley, "Photonic analog-to-digital converters," *Opt. Exp.*, vol. 15, no. 5, pp. 1955–1982, Mar. 2007.

[7] A. Khilo et al., "Photonic ADC: Overcoming the bottleneck of electronic jitter," *Opt. Exp.*, vol. 20, no. 4, pp. 4454–4469, Feb. 2012.

[8] D. Marpaung et al., "Integrated microwave photonics," *Laser Photon. Rev.*, vol. 7, no. 4, pp. 506–538, Jan. 2013.

[9] Q. Zhang et al., "Linearity comparison of silicon carrier-depletion-based single, dual-parallel, and dual-series Mach–Zehnder modulators," *J. Lightw. Technol.*, vol. 36, no. 16, pp. 3318–3331, Aug. 2018, doi: 10.1109/JLT.2018.2839603.

[10] Y. Zhou, L. Zhou, F. Su, X. Li, and J. Chen, "Linearity measurement and pulse amplitude modulation in a silicon single-drive push–pull Mach–Zehnder modulator," *J. Lightw. Technol.*, vol. 34, no. 14, pp. 3323–3329, Jul. 2016.

[11] M. Streshinsky et al., "Highly linear silicon traveling wave Mach-Zehnder carrier depletion modulator based on differential drive," *Opt. Exp.*, vol. 21, pp. 3818–3825, Feb. 2013.

[12] Y. Zhou et al., "Linearity characterization of a dual–parallel silicon Mach–Zehnder modulator," *IEEE Photon. J.*, vol. 8, no. 6, Dec. 2016, Art. no. 7805108, doi: 10.1109/JPHOT.2016.2616488.

[13] J. Ding, S. Shao, L. Zhang, X. Fu, and L. Yang, "Method to improve the linearity of the silicon Mach-Zehnder optical modulator by doping control," *Opt. Exp.*, vol. 24, pp. 24641–24648, 2016.

[14] A. M. Gutierrez et al., "Analytical model for calculating the nonlinear distortion in silicon-based electro-optic Mach–Zehnder modulators," *J. Lightw. Technol.*, vol. 31, no. 23, pp. 3603–3613, Dec. 2013, doi: 10.1109/JLT.2013.2286838.

[15] C. G. Bottenfield, V. A. Thomas, and S. E. Ralph, "Silicon photonic modulator linearity and optimization for microwave photonic links," *IEEE J. Sel. Top. Quantum Electron.*, vol. 25, no. 5, Sep./Oct. 2019, Art. no. 3400110, doi: 10.1109/JSTQE.2019.2908784.

[16] Y. Zhou et al., "Modeling and optimization of a single-drive push–pull silicon Mach–Zehnder modulator," *Photon. Res.*, vol. 4, pp. 153–161, Aug. 2016.

[17] H. Yu and W. Bogaerts, "An equivalent circuit model of the traveling wave electrode for carrier-depletion-based silicon optical modulators," *J. Lightw. Technol.*, vol. 30, no. 11, pp. 1602–1609, Jun. 2012, doi: 10.1109/JLT.2012.2188779.

[18] A. Samani et al., "Experimental parametric study of a silicon photonic modulator enabled 112-gb/s PAM transmission system with a DAC and ADC," *J. Lightw. Technol.*, vol. 33, no. 7, pp. 1380–1387, Apr. 2015.

[19] D. Frickey, "Conversions between S, Z, Y, H, ABCD, and T parameters which are valid for complex source and load impedances," *IEEE Trans. Microw. Theory Tech.*, vol. 42, no. 2, pp. 205–211, Feb. 1994.

[20] D. Patel et al., "Design, analysis, and transmission system performance of a 41 GHz silicon photonic modulator," *Opt. Exp.*, vol. 23, pp. 14263–14287, Jun. 2015.

[21] H. Xu, X. Li, X. Xiao, Z. Li, Y. Yu, and J. Yu, "Demonstration and characterization of high-speed silicon depletion-mode Mach–Zehnder modulators," *IEEE J. Sel. Top. Quantum Electron.*, vol. 20, no. 4, Jul./Aug. 2014, Art. no. 3400110, doi: 10.1109/JSTQE.2013.2293763.

[22] H. Chen, "Development of an 80 gbit/s InP-based Mach–Zehnder modulator," Ph.D. dissertation, Dept. Elect. Eng. Comput. Sci., Tech. Univ., Berlin, Germany, 2007.

[23] W. B. Bridges and J. H. Schaffner, "Distortion in linearized electrooptic modulators," *IEEE Trans. Microw. Theory Techn.*, vol. 43, no. 9, pp. 2184–2197, Sep. 1995, doi: 10.1109/22.414563.

Min-Hyeok Seong (Graduate Student Member, IEEE) received the B.S. degree in electrical and electronic engineering, in 2019 from Yonsei University, Seoul, South Korea, where he is working toward the combined Ph.D. degree with High-Speed Circuits and Systems Laboratory. His current research focuses on several research topics, including optical modulators based on Si photonics for digital and analog applications.

Yongjin Ji received the B.S. degree in electrical and electronic engineering from Yonsei University, Seoul, South Korea, in 2020. He is currently with High-Speed Circuits and Systems Laboratory, Yonsei University. His research interests include designing and optimizing Si photonic optical devices for various applications.

Chul-Soon Im received the B.S., M.S., and Ph.D. degrees from the Department of Electronic Engineering, Kwangwoon University, Seoul, South Korea, in 2015, 2017, and 2021, respectively. Since 2021, he has been with the Hanwha Systems Company, Ltd, Yongin R&D Center, Gyeonggi-do, South Korea. His research focuses on several research topic, including microwave photonic integrated circuits and photonic radars.

Youngseok Bae received the M.S. degree in electrical engineering from Korea University, Seoul, South Korea, in 2011, and the Ph.D. degree from the Korea Advanced Institute of Science and Technology, Daejeon, South Korea, in 2021, respectively. Since 2011, he has been a Senior Researcher with the Agency for Defense Development, Daejeon. His research interests include photonic analog-to-digital converter, silicon photonics, and microwave photonic radar.

Woo-Young Choi (Member, IEEE) received the B.S., M.S., and Ph.D. degrees in electrical engineering and computer science from the Massachusetts Institute of Technology, Cambridge, MA, USA, in 1986, 1988, and 1994, respectively. His doctoral dissertation concerned the investigation of molecular-beam epitaxy grown InGaAlAs laser diodes for fiber-optic applications. From 1994 to 1995, he was a Postdoctoral Research Fellow with NTT Opto-Electronics Laboratories, where he worked on femtosecond all-optical switching devices based on low-temperature grown InGaAlAs quantum wells. In 1995, he joined the Department of Electrical and Electronic Engineering, Yonsei University, Seoul, South Korea, where he is currently a Professor. His research interests include high-speed circuits and systems that include high-speed optoelectronics, high-speed electronic circuits, and silicon photonics.